Revision 1

Crystal structures of laihunite and intermediate phases between laihunite-1M and fayalite: Z-contrast imaging and *ab initio* study

Huifang Xu[1*], Zhizhang Shen[1], Hiromi Konishi[1], Pingqiu Fu[2], and Izabela Szlufarska[3]

[1]NASA Astrobiology Institute, Department of Geoscience,
University of Wisconsin - Madison
Madison, Wisconsin 53706, USA

[2]Institute of Geochemistry
Science Academy of China
Guiyang, Guizhou 550002, P. R. China

[3]Department of Materials Science and Engineering,
University of Wisconsin-Madison,
Madison, Wisconsin 53706, USA

* Corresponding author: Dr. Huifang Xu
Tel: 1-608-265-5887
Fax: 1-608-262-0693
Email: hfxu@geology.wisc.edu

ABSTRACT

Crystals of laihunite from Xiaolaihe of Liaoning Province, NE China, were studied using selected-area electron diffraction (SAED), high-resolution transmission electron microscopy (HRTEM), and Z-contrast imaging. Z-contrast images directly reveal ordered vacancies in M1 sites. The results confirm early structural models for 1-layer laihunite (or laihunite-1M) with ideal stoichiometry of $[]_{0.5}Fe^{2+}_{0.5}Fe^{3+}SiO_4$. 2-layer laihunite and 3-layer laihunite are found to be chemically different from laihunite-1M. The 2-layer laihunite can be viewed as a periodic intergrowth of laihunite and fayalite in the 1:1 ratio. The 3-layer laihunite can be considered to be a periodic intergrowth of laihunite and fayalite in the 1:0.5 ratio along the ***c***-axis. Ideal stoichiometries for the 2-layer structure and the 3-layer structure are $[]_{0.5}Fe^{2+}_{2.5}Fe^{3+}[SiO_4]_2$, and $[]_{1.0}Fe^{2+}_{3.0}Fe^{3+}_{2.0}[SiO_4]_3$, respectively. The structural intergrowth of the 3-layer laihunite and the 1-layer lahunite results in chemical compositions falling within the range between the two aforementioned structures, such as the chemical formula of $[]_{0.4}Fe^{2+}_{0.8}Fe^{3+}_{0.8}SiO_4$, reported earlier in literatures.

The crystal structures of the 1-layer laihunite (1M), the 2-layer laihunite (2M), and the 3-layer laihunite (3Or) determined from Z-contrast images and *ab initio* calculations using the density functional theory (DFT) have space groups of $P2_1/b$, $P2_1/b$, and *Pbnm*, respectively. The previously reported monoclinic symmetry for the 3-layer laihunite may be an artifact due to overlapping diffraction spots from both, the laihunite-3Or and the laihunite-1M. Our study demonstrates that the method of combining Z-contrast imaging and *ab initio* calculation can be effectively used for identifying structures of nano-phases in host crystals.

INTRODUCTION

Laihunite that has a distorted olivine-type structure with ferric and ferrous irons and ordered distribution of vacancies was first discovered in a high-grade metamorphosed banded iron formation (BIF) (Laihunite Research Group, 1976; Fu et al., 1982). The occurrence of laihunite is not limited to metamorphosed BIFs. Laihunite was also found in certain black fayalite (Schaefer, 1983; 1985), some ferric-fayalite from granite, and Fe-bearing olivine from volcanic and intrusive rocks (Sueno et al., 1985; Banfield et al., 1990, 1992; Janney and Banfield, 1998; Putnis, 1979; Xu et al., 1992; Konishi and Xu, 2012). The laihunite, which coexists with fayalite, magnetite, quartz, ferrosilite, almandine and hedenbergite, was formed in the process of oxidation of fayalite during metamorphism (Fu et al., 1982; Wang, 1982; Kitamura et al., 1984). The structure refinement of the 1-layer laihunite shows $P2_1/b$ symmetry and ordered arrangement of vacancies in half of the M_1 sites of a fayalite structure (Fu et al., 1982). A proposed ideal structural formula for the 1-layer laihunite is $[]_{0.5}Fe^{2+}_{0.5}Fe^{3+}SiO_4$ (Fu et al., 1982). However, structural details regarding symmetry and the number of vacancies in the structures are still a matter of controversy (Fu et al., 1982; Tamada et al., 1983; Ferrifayalite Research Group, 1976). To address these questions, it was proposed that the 1-layer structure is an average of the 3-layer laihunite that has a tripled periodicity along the ***c***-axis with respect to fayalite structure (Shen et al., 1984; Tamada et al., 1983). A recent *ab initio* calculation result even suggested that 1-layer laihunite structure may have a triclinic symmetry (Chatterjee and Saha-Dasgupta, 2010).

Transmission electron microscopy (TEM) and some X-ray studies have shown that there are also domains of fayalite, the 3-layer, and the 2-layer structures that are intergrown with

laihunite (Li et al., 1981; Fu et al., 1982; Kitamura et al., 1984; Sueno et al., 1985; Chou, 1985; Kondoh et al., 1985). Single-crystal structure refinement of a 3-layer laihunite was carried out based on $P2_1/b$ symmetry (Shen et al., 1982; 1984). It was found that a 3-layer laihunite synthesized by oxidizing fayalite at high temperature has a higher Fe content than natural 2-layer and 3-layer laihunite structures do (Kondoh et al., 1985). At the same time, the synthetic 3-layer structure is different from the natural 3-layer laihunite in composition (Kondoh et al., 1985). All the reported TEM data suggest intergrowth of the laihunite structures at nanometer and sub-micrometer scales (1-layer, 2-layer, and 3-layer domains). Proposed models for the 3-layer laihunite superstructure are also controversial regarding the number of vacancies and the distributions of vacancies (Li et al., 1981; Shen et al., 1984; Chou, 1985). A 3-layer laihunite structure with monoclinic symmetry determined using X-ray single crystal diffraction method was proposed based on observation of overlapping diffraction peaks from multiple phases with the average composition of $[]_{0.4}Fe^{2+}_{0.8}Fe^{3+}_{0.8}SiO_4$ (Shen et al., 1984). In this paper, we use state-of-the-art methods of high-resolution Z-contrast imaging, in-situ X-ray EDS analyses, and *ab initio* calculation based on the density function theory (DFT) method to provide both structures and compositions of the laihunite (laihunite-1M) and intermediate phases between laihunite-1M and fayalite.

SAMPLE AND EXPERIMENT

Samples for TEM and associate X-ray energy-dispersive spectroscopy (EDS) investigation of laihunite crystals were obtained from Xiaolaihe, Liaoning Province, NE China, where in fact the laihunite was first discovered. The host rock of the above minerals is Archean

metamorphosed BIF. Other coexisting minerals are fayalite, laihunite, magnetite, quartz, ferrosilite and hedenbergite (Laihunite Research Group, 1976; Ferrifayalite Research Group, 1976).

Our first TEM experiments were carried out with a Philips 420ST electron microscope equipped with an EDAX energy-dispersive X-ray spectrometer and a Princeton Gamma-Tech System-4000 analyzer as that described by Livi and Veblen (1987). Transmission electron microscopy and scanning transmission electron microscopy (STEM) studies were carried out using a FEI Titan 80-200 aberration corrected scanning/transmission electron microscope operated at 200 kV coupled with an EDAX high resolution EDS detector and Gatan image filtering system. This instrument is capable of imaging single atoms with ~ 0.1 nm spatial resolution in STEM mode. Probe current was set at 24.5 pA. Collection angle of HAADF detector for acquiring all the Z-contrast images ranges from 54 to 270 mrad (corresponding to 7.5 (1/Å) to 38.2 (1/ Å) in reciprocal space).

The scanning transmission electron microscopy (STEM) method uses the high-angle annular dark-field (HAADF) detector to give the most highly localized 1s Bloch state imaging, which eliminates most of the obvious effects of dynamical diffraction. Z-contrast images are HAADF images with atomic resolution (Kirkland, 1998). The intensity of Z-contrast images is dependent on numbers of atoms (n) in an atomic column (or occupancy) and atomic number of atoms in the sites through ~ $\mathbf{Z^2}$ (Pennycook, 2002). Local composition and occupancy may be obtained from measured intensities. The relationship between intensity and atomic number for

the experimental condition based on calculated intensities for atoms columns in a Co-Mn-Si alloy is ~ $\mathbf{Z}^{2.27}$ (Shi, 2013).

Specimens for TEM/STEM investigation were prepared by crushing the selected crystals in alcohol and then depositing a drop of crystal suspension on holy-carbon Cu-grids. Because of fairly well developed {100} and {010} cleavages of fayalite and laihunite, it is not difficult to get crystal grains containing 00*l* diffraction in their diffraction patterns. Fayalite (Fe_2SiO_4) and forsterite (Mg_2SiO_4) were used as a standard for determination of the K-factor of Fe and Mg. All settings for the X-ray energy dispersion spectra (EDS) collections were the same as for the K-factor determination. Fe^{2+} and Fe^{3+} of the laihunite were calculated from the (Fe+Mg+Mn+Ca+Ni)/Si ratio deduced from the EDS results, by considering charge balance and assuming all tetrahedral sites are occupied by Si. X-ray EDS analysis from a small area with known structure can be obtained by combining selected area electron diffraction (SAED) and HRTEM images collected from the same area. This analysis is possible because SAED and HRTEM can provide structural information from very small areas, such as domains of 1-layer laihunite, 2-layer laihunite, and 3-layer laihunite.

The DFT calculations were performed by using Vienna *Ab Initio* Simulation Package (VASP) (Kresse et al., 1996). The general gradient approximation (GGA) with the Perdew, Burke, and Ernzerhof (PBE) parameters was employed (Perdew et al., 1996). The projector-augmented wave (PAW) method with the energy cutoff of 600 eV was used. K-point meshes of 4×4×2, 4×2×2, and 4×1×2 were found to be sufficient for 1-layer, 2- layer, and 3-layer laihunite structures, respectively. In order to take into account the on-site Coulomb repulsion of 3d

electron in Fe atoms, we employed a simplified (rotationally invariant) approach known as GGA+U (Dudarev et al., 1998). In Dudarev's method, an effective U parameter, $U_{eff} = U-J$, is used. According to previous DFT calculations of fayalite (Cococcioni et al., 2003; and Stackhouse et al., 2010), Ueff=4.8eV is a reasonable value and thus it was used in this study. All initial structures with P1 symmetry proposed in this study were relaxed using the static energy minimization scheme, where both the shape and volume of the cell were allowed to relax. The final structures with lowest energy states are chosen as possible structures for the 3 phases. The electron diffraction patterns of calculated structures were generated by SingleCrystal™ software.

RESULTS AND DISCUSSIONS

TEM results

TEM images show that the crystals are heterogeneous in structure with nano-cracks between neighboring domains (Figure 1). Selected-area electron diffraction (SAED) patterns show that the crystal contains laihunite (or 1-layer laihunite), 3-layer laihunite domains, 2-layer laihunite domains, and fayalite domains (Figure 2). We found many areas with intergrown 3-layer and 1-layer laihunite structures (Figure 2D, 2E). The SAED pattern (E) shows diffractions from 1-layer laihunite and 3-layer laihunite. Positions of 001 and 003 are not from the 3-layer laihunite domain, but from 1-layer laihunite domain, because they are off the center between 00 2/3 and 00 4/3, and between 00 8/3 and 00 10/3 reflections (fractional indices are based on fayalite unit cell and setting). Periodicity along the ***c***-axis for the 3-layer laihunite is 1.5***c*** of the 1-layer laihunite. Diffraction spots of 001 and 003 from a 1-layer laihunite should not be considered as 003 and 009 diffractions of the 3-layer laihunite structure. Unit cell parameters can

be measured by comparing the diffraction difference and Fast Fourier transform (FFT) patterns between known structure (fayalite) and unknown laihunite phases with different periodicities along their ***c***-axes (Table 1).

X-ray EDS spectra of laihunite with different structures (different periodicities along the ***c***-axis) were collected from relatively ordered domains and confirmed by SAED patterns and HRTEM images. Using a general formula for laihunite $[]_xFe^{2+}_{2-3x}Fe^{3+}_{2x}SiO_4$, we found the number of vacancies for the 1-layer laihunite range from 0.47-0.52; the amount of vacancies for the 3-layer laihunite range from 0.30-0.39; and the amount of vacancies for the 2-layer laihunite range from 0.21-0.25. The observed laihunite domains with difference periodicities are chemically distinct (Table 2), and they are not in simple substructure and superstructure relationships.

Z-contrast imaging results

Z-contrast image of a fayalite area shows the positions of Fe (bright spots) and Si (much less bright spots among 3 Fe atoms). A structure model of fayalite is also overlaid on the image. Positions of oxygen are omitted for clarity because scattering from oxygen atom is much weaker than those from Fe and Si atoms. The diffraction spots of *00l* (*l*=odd) appear in SAED pattern (Figure 2C) and FFT pattern (Figure 4C) from fayalite due to multiple diffraction of coherent scattered electrons at low-angle. Z-contrast images that use the high-angle annular dark-field (HAADF) detector to collect non-coherent scattered electrons at high angle eliminate most of the obvious effects of dynamical diffraction (Pennycook, 2002). FFT pattern from the Z-contrast

image of Figure 3 does not show 001, 003 spots due to 2-fold screw axis along the ***c***-axis in fayalite structure (Figure 4D).

A [100]-zone-axis Z-contrast image at the interface between fayalite and laihunite shows Fe vacancies at M1 sites within some of the (001) planes. Periodic distribution of the vacancies results in locally ordered domains of 2-layer laihunite (labeled 2) and 3-layer laihunite (labeled 1.5) (Fig. 5). A [110]-zone-axis Z-contrast image shows intergrowth of 1-layer laihunite, 2-layer laihunite, and 3-layer laihunite domains (Fig. 6). The Z-contrast images directly show positions of Fe vacancies in some of the M1 sites of fayalite-based structure. Structure models for 1-layer, 2-layer and 3-layer laihunite can be obtained based on observed distribution of vacancies in fayalite-based structure. Figure 7 is a [100]-zone-axis Z-contrast image of 1-layer laihunite domain. Half of the M1 sites are vacancies in the 1-layer laihunite. Structure model for the 1-layer laihunite is also overlaid on the original image (Fig. 7A) and the noise-filtered image (Fig. 7B). The structure of the 1-layer laihunite is found to have a monoclinic symmetry. Some areas show a twin relationship between neighboring 1-layer laihunite domains and interface between 1-layer and 3-layer laihunite (Figure 8). Stoichiometry for the 1-layer laihunte domains is $[]_{0.5}Fe^{2+}_{0.5}Fe^{3+}SiO_4$ based on the number of vacancies in half of the M1 sites. Fe in M2 site neighboring the vacancies will be ferric Fe in order to maintain the local charge balance. This assertion is consistent with chemical compositions found by analyzing laihunite-1M domains (Table 2).

A [110]-zone-axis Z-contrast image from an area dominated by 3-layer laihunite shows that (001) vacancy layers occur every one and half fayalite units along the ***c***-axis. Periodicity

along the ***c***-axis is tripled with respect to the fayalite structure (Figure 9). FFT pattern from the image shows 002, and 004 spots, which indicates a 2-fold screw axis along the ***c***-axis of the 3-layer laihunite structure. The 3-layer laihunite will keep orthorhombic symmetry (or, laihunite-3Or). Stoichiometry for the laihunite-3Or will be $[]_{1.0}Fe^{2+}_{3.0}Fe^{3+}_{2.0}[SiO_4]$. This is consistent with chemical compositions from analyzed laihunite-3Or domains (Table 2). The structural intergrowth of 3-layer laihunite and 1-layer laihunite will results in chemical compositions that lie between the ideal 1-layer laihunite and 3-layer laihunite, such as the reported chemical formula of $[]_{0.4}Fe^{2+}_{0.8}Fe^{3+}_{0.8}SiO_4$ (Shen et al., 1984).

DFT CALCULATIONS

Z-contrast images provide structure models that are based on compositions and distributions of vacancies among the M1 sites of fayalite-based structure. In order to obtain detailed atomic positions for the proposed structure models, we carried out *ab initio* calculation using DFT. In these calculations, it is important to consider magnetic properties of Fe in a given structure. According to published data, there are two possible antiferromagnetic (AF) configurations of fayalite: AF interaction between edge-sharing octahedra and AF interaction between corner-sharing octahedra (Cococcioni et al., 2003). In DFT calculations of 1-layer laihunite (Chatterjee and Saha-Dasgupta, 2010), the latter configuration was found to have a lower energy. Our calculations confirm that the latter configuration is more stable for all three laihunite structures (see appendix). Therefore, the laihunite structures reported below were calculated using the second magnetic configuration.

227 The distributions of vacancies in the initial structure models were based on the STEM
228 observation that all vacancies occupy the M1 sites of fayalite-based structure. The optimized
229 configurations with lowest energy for 1-layer, 2-layer and 3-layer laihunite structures are shown
230 in Figures 10 and 11. A monoclinic structure model (laihunite-3M) based on Shen et al., (1984)
231 is also illustrated for comparison. Obviously, the "laihunite-3M" model does not fit observed Z-
232 contrast images. The unit cell parameters calculated from DFT are reported in Table 1 and they
233 show a good agreement with the experimentally measured values. Because of the vacancy
234 positions, the symmetries of 1-layer and 2-layer laihunite structures are reduced to monoclinic
235 (the alpha angle are 91.39˚ and 90.79˚, respectively), whereas 3-layer laihunite structure retains
236 the orthorhombic symmetry. The 1-layer and 2-layer laihunite structures have space group $P2_1/b$
237 (no. 14) (Table 3). The 3-layer laihunite structure resumes the same space group of *Pbnm* (no.
238 62) as fayalite (Table 3). Here, we use laihunite-1M, laihunite-2M, and laihunite-3Or to
239 represent the observed 1-layer, 2-layer, and 3-layer laihunite structures, although they are not
240 polymorphs with the same composition.
241
242 In laihunite-1M, the M1-O_6 octahedra are larger than the M2-O_6 octahedra. In addition,
243 the M2-O_6 octahedra are slightly more distorted (Table 4), which is consistent with conclusions
244 from earlier calculations, although the earlier calculations suggest a triclinic symmetry for the 1-
245 layer laihunite (Chatterjee and Saha-Dasgupta, 2010). Comparing all the structure models with
246 fayalite structure, the positions for Si and Fe2 are shifted away from their ideal positions in
247 fayalite (fractional coordinate z=0,25 for Si and Fe2), because of the presence of Fe(III) in those
248 Fe2 sites that neighbor the vacancies (Table 5). However, fractional coordinates for Si and Fe2 in
249 all the reported structures are different (Table 5). Our calculated structure shows that both Fe2

and Si atoms are slightly shifted towards vacancy sites, instead of opposite shifts along the ***c***-axis with respect the Si and Fe positions in fayalite structure.

For laihunite-2M we find that, while there are similar M1-O_6 and M2-O_6 (Fe^{3+}-O_6) octahedra adjacent to the vacancies as in laihunite-1M, the octahedra away from vacancies resemble those in fayalite. The laihunite-2M domains will also form twins, similarly to those observed in laihunite-1M.

In laihunite-3Or, there is just one type of M1-O_6 octahedra due to its orthorhombic symmetry (Table 4). The calculated laihunite-3Or structure is different from a previously proposed structure with monoclinic symmetry (Shen et al., 1984). The laihunite crystals contain nanometer to sub-micrometer scales of domains of all 3 laihunite structures and even residual fayalite. The crystal analyzed by She et al. (1984) contains domains of laihunite-1M and laihunite-3Or. X-ray diffraction peaks from the crystal will overlap with peaks from laihunite-1M and laihunite-3Or. If odd *00l* reflections from laihunite-1M are considered as 003 and 009 reflections (based on 3-layer laihunite setting), the obtained structure will have a monoclinic symmetry ($P2_1/b$) instead of an orthorhombic symmetry (*Pbnm*). Structural intergrowth of 3-layer laihunite and 1-layer lahunite will result in average chemical compositions between the laihunite-1M and laihunite-3Or. The reported formula of $[]_{0.4}Fe^{2+}_{0.8}Fe^{3+}_{0.8}SiO_4$ (Shen et al., 1984) is an average composition of laihunite-1M and laihunite-3Or.

Chou (1985) proposed 2 types of 3-layer laihunite structures based on HRTEM images from [110]-zone-axis (for $3C_1$ structure odd and even 0*0l* reflections) and [010]-zone axis (for $3C_2$ structure with even *00l* reflections). According to our Z-contrast images and calculated structure (*Pbnm*) for the laihunite-3Or, odd *00l* reflections and tripled periodicity along the ***c***-axis in [110]-zone-axis SAED pattern and high-resolution transmission electron microscopic (HRTEM) images may be artifacts from multiple diffractions. In [010]-zone-axis SAED pattern and HRTEM image, there will be no odd 00l reflections due to *n*-glide plane perpendicular to (010). There is only one type of 3-layer structure, i.e., laihunite-3Or.

The observed 2-layer and 3-layer structures are not simple superstructures of laihunite-1M, because their compositions are different from that of laihunite-1M. The originally proposed laihunite structure has 1-layer periodicity with ideal stoichiometry of $[]_{0.5}Fe^{2+}_{0.5}Fe^{3+}SiO_4$ (Laihunite Research Group, 1976; Fu et al., 1982). The observed intermediate phases are very similar to those in mixed-layer clay minerals, such as interstratified chlorite/serpentine minerals (Banfield and Bailey, 1996; Xu and Veblen, 1996). The observed intermediate structures in the laihunite – fayalite system and forsterite – Mg-laihunite system may be also described as interstratified olivine / laihunite minerals.

We propose that the observed laihunite structures are stable only within the fayalite host and we propose the following scenario for formation of these structures. Generally, the laihunite domains are formed during oxidative reaction of the fayalite in the solid state. Domains formed in early stage contain fewer vacancies and they serve as host phases to stabilize domains formed

294 at later stages and with more vacancies. The reactions for the laihunitization of fayalite may be
295 simplified as

296 $2Fe_2SiO_4 + 0.125O_2 \rightarrow 2[]_{0.25}Fe^{2+}_{1.25}Fe^{3+}_{0.5}SiO_4 + 0.25Fe^{2+}$.

297 fayalite laihunite-2M

298

299 $2[]_{0.25}Fe^{2+}_{1.25}Fe^{3+}_{0.5}SiO_4 + 0.15O_2 \rightarrow 2[]_{0.33}Fe^{2+}_{1.0}Fe^{3+}_{0.67}SiO_4 + 0.3Fe^{2+}$.

300 laihunite-2M laihunite-3Or

301

302 $2[]_{0.33}Fe^{2+}_{1.0}Fe^{3+}_{0.67}SiO_4 + 0.1O_2 \rightarrow 2[]_{0.5}Fe^{2+}_{0.5}Fe^{3+}_{1.0}SiO_4 + 0.2Fe^{2+}$.

303 laihunite-3Or laihunite-1M

304

305 Extra Fe, generated as a product of the above reactions, diffuses out of the lattice and precipitates
306 as magnetite at some tunnels areas (Figs. 1 and 12). Formation of laihunite results in shrinking of
307 the unit cells, especially along the ***c***-axis (Table 1) and in formation of nano-tunnels or cracks
308 that parallel to (001). The net reaction for the laihunitization of fayalite can be written as

309 $6Fe_2SiO_4 + 2O_2 \rightarrow 6[]_{0.5}Fe^{2+}_{0.5}Fe^{3+}_{1.0}SiO_4 + Fe_3O_4$.

310 fayalite laihunite-1M magnetite

311

312 The migration of oxygen and iron ions may be enhanced in the presence of fluid phase through
313 the nano-crack and tunnels within the crystal (Fig. 12). Magnetite nano-precipitates occur at
314 some nano-tunnels. Observed epitaxial relationship between the magnetite precipitates and
315 laihunite host is one of magnetite {111} ~ // {100} of laihunite, and one of magnetite {110} ~ //
316 (001) of laihunite.

IMPLICATIONS

It is very challenging to solve crystal structures of nano-precipitates in host minerals using X-ray diffraction and TEM. Our results provide a new way for solving the crystal structures of nano-crystals in or intergrown with host minerals, and locally ordered domains in interstratified clay minerals. Z-contrast imaging can provide information about topology of the crystal structure, and DFT calculation provides accurate coordinates of the atoms within a unit cell. The observed vacancy ordering in Fe-rich olivine may provide information about highly anisotropic diffusion of atoms in Fe^{3+}-bearing olivine crystals. Vacancy layers in Fe^{3+}-bearing olivine may behave as a "highway" for atom diffusion. Z-contrast imaging is a powerful tool for direct observation of vacancies and other defects. The method can be used for studding oxidation of iron and vacancy ordering in other minerals, such as Fe-bearing olivine minerals, and chain silicate minerals, and Fe-bearing oxide minerals. The combination of complementary methods described in this paper can be used for observing and quantifying local ordering of Fe atoms and vacancies in partially oxidized Mg-rich olivine crystals reported by Janney and Banfield (1998) and Konishi and Xu (2012).

ACKNOWLDEGEMENTS

This work is supported by NASA Astrobiology Institute (N07-5489) and NSF (EAR-095800). Authors thank Dr. Alex Kivit for optimizing instrument condition. Author also thank Major Research Instrumentation (MRI) program of NSF for funding the aberration corretced STEM. Xu thanks Prof. David Veblen for supporting his early TEM works at Johns Hopkins University.

REFERENCES

Banfield, JF, Dyar, MD, and McGuire, AV (1992) The defect microstructure of oxidized mantle olivine from Dish Hill, California. American Mineral 77: 977-986.

Banfield, JF, Veblen, DR and Jones BF (1990) Transmission electron microscopy of subsolidus oxidation and weathering of olivine. Contrib. Mineral. Petrol 106: 110-123.

Banfield, JF, and Bailey, SW (1996) Formation of regularly interstratified serpentine – chlorite minerals by tetrahedral inversion in long-period serpentine polytypes. American Mineralogist, 81, 79-81.

Chatterjee, S, and Saha-Dasgupta, T (2010) First-principles simulations of structural, electronic, and magnetic properties of vacancy-bearing Fe silicates. Physical Review B, 81, 155105

Chou, BS (1985) Fine textures in silicate minerals. in K. H. Kuo and H. Q. Ye ed., "High-Resolution Electron Microscopy" (in Chinese), Science Press, Beijing, pp 423-445.

Cococcioni, M, Corso, AD, and de Gironcoli, S (2003) Structural, electronic, and magnetic properties of Fe_2SiO_4 fayalite: Comparison of LDA and GGA results. Physical Review B, 67, 094106.

Dudarev, SL, Botton, GA, Savrasov, SY, Humphreys, CJ and Sutton, AP (1998) Electron-energy-loss spectra and the structural stability of nickel oxide: An LSDA+U study. Physical Review B, 57, 1505-1509.

Ferrifayalite Research Group, Department of Geology of Peking University and Institute of Geology and Mineral Resources of Chinese Academy of Geological Sciences (1976) Ferrifayalite and its crystal structure. Acta Geologica Sinica. 2, 161-175 (in Chinese).

Fu, P Kong, Y and Zhang, L (1982) Domain twinning of laihunite and refinement of its crystal structure. Chinese Journal of Geochemistry 1: 115-133.

Fujino, K, Sasaki, S, Takeuchi, Y, and Sadanaga, R (1981) X-ray determination of electron distributions in forsterite, fayalite and tephroite. Acta Crystallographica B37: 513-518

Janney, D E, and Banfield, JF (1998) Distribution of cations and vacancies and the structure of defects in oxidized intermediate olivine by atomic-resolution TEM and image simulation. American Mineral., 83: 799-810.

Kirkland, E.J. (2010) Advanced computing in electron microscopy. Plenum Press, New York, 250 pp.

Kitamura, M, Shen, B, Banno, S and Morimoto, N (1984) Fine texture of laihunite, a nonstoichiometric distorted olivine-type minerals. American Mineral 69: 154-160.

Kohlstedt, DL, Vander Sande, JB (1975) An electron microscopy study of naturally occurring oxidation produced precipitates in iron-bearing olivines. Contrib Mineral. Petro 53: 13-24.

Kondoh, S, Kitamura, M and Morimoto, N (1985) Synthetic laihunite ($[]_xFe^{2+}_{2-3x}Fe^{3+}_{2x}SiO_4$), an oxidation product of olivine. American Mineral 70: 737-746.

Konishi, H and Xu, H (2012) Direct observation of vacancies and iron atoms in a Mg-rich olivine using Z-contrast imaging, Microscopy and Microanalysis, 18, Supplement S2, 348-349.

Kresse, G, and Furthmüller, J (1996) Efficiency of ab-initio total energy calculations for metals and semiconductors using a plane-wave basis set. Computational Materials Science, 1, 15-50.

Laihunite Research Group (1976) Laihunite -- a new iron silicate mineral (in Chinese). Geochimica 2: 95-103.

Li, H, Liu, W, Kong, Y and Fu, P (1981) The lattice fringes of laihunite (in Chinese). Kexue Tongbao 10: 590-592.

Livi, KJT and Veblen, DR (1987) “Eastonite” from Easton, Pennsylvania; A mixture of phlogopite and a new form of serpentine. American Mineral 72: 113-125.

Pennycook, S (2002) Structure determination through Z-contrast microscopy. Advances in imaging and electron physics, 173-206.

Perdew, JP, Burke, K and Ernzerhof, M (1996) Generalized gradient approximation made simple. Physical Review Letters, 18, 3865-3868.

Putnis, A (1979) Electron petrography of high-temperature oxidation in olivine from Rhum layered intrusion. Mineral Mag 43: 293-296.

Schaefer, MW (1983) Measurements of iron (III)-rich fayalites. Nature 303: 325-327.

Schaefer, MW (1985) Site occupancy and two-phase character of "fayalite". American Mineral 70: 729-736.

Shen, B, Tamada, O, Kitamura, M and Morimoto, N (1982) The superstructure of laihunite ($Fe^{2+}_{0.5}Fe^{3+}_{1.0}SiO_4$) (in Chinese). Scientia Giologica Sinica 3: 341-342.

Shen, B, Tamada, O, Kitamura, M and Morimoto, N (1984) Superstructure of laihunite-3M ($[]_{0.4}Fe^{2+}_{0.8}Fe^{3+}_{0.8}SiO_4$). American Mineral 71: 1455-1460.

Shi, F (2013) Advanced electron microscopy of novel ferromagnetic materials and ferromagnet / oxide interfaces in magnetic tunnel junctions. Ph. D. Dissertation, University of Wisconsin - Madison.

Stackhouse, S, Stixrude, L, and Karki, BB (2010) Determination of the high-pressure properties of fayalite from first-principles calculations. Earth and Planetary Science Letters, 289, 449-456

Sueno, S, Matsuura, S, and Prewitt CT (1985) Fe-deficient olivine structure type minerals from Colorado, U. S. A. and Japan. Mineralogical Journal (Japan) 12: 376-392.

Tafto, J Spence, J (1982) Crystal site location of iron and trace elements in an Mg-Fe-olivine using a new crystallographic technique. Science 218: 49.

Tamada, O, Shen, B, and Morimoto, N (1983) The crystal structure of laihunite (([]0.4Fe2+0.8Fe3+0.8SiO4). Mineralogical Journal, 11, 382-391.

Xu, HF, Xu, HW, and Luo, G (1992) Domain structures in minerals. Science in China 35B: 1218-1223 with plates I & II.

Xu, H, and Veblen, DR (1996) Interstratification and other reaction microstructures in the chlorite-berthierine series. Contribution to Mineralogy and Petrology, 124, 291-301.

Figure captions

Figure 1: (A) TEM image showing a structural heterogeneity of a laihunite crystal with nano-cracks or nano-tunnels (indicated by arrows) between neighboring domains. Nano-cracks formed during the transformation from fayalite to laihunite due to the difference in the ***c***-dimensions between fayalite and laihunite. Inserted FFT pattern shows streaking along the ***c**** direction and intensity maxima at 00 ½ and 00 2/3 positions (indicated by 2 short arrows). (B) An HRTEM image showing intergrowth of 2-layer and 3-layer laihnunite domains and nano-tunnels.

Figure 2: SAED patterns from 3-layer laihunite (A), intergrown 2-layer and 3-layer laihunite (B), intergrown fayalite and 2-layer laihunite (C), [010]-zone axis of intergrown 1-layer and 2-layer laihunite (D), and tilted crystal with only *00l* reflections to avoid multiple diffraction from *hkl* spots (E).
Al the indices are based on fayalite unit cell setting. Arrows in (A) indicate extra spots from tripled periodicity along the ***c***-axis. Long arrows and short arrows in (B) indicate diffraction spots from 3-layer laihunite and 2-layer laihunite, respectively. SAED (C) shows splitting in high order *00l* reflections (005, 006) from fayalite and the 2-layer laihunite domain. All the indices are based on fayalite setting.

Figure 3: Z-contrast image of fayalite ([100]-zone axis) shows positions of Fe in M1 and M2 sites. Fayalite model is also overlaid on the image. Si atoms at the center among 3 Fe atoms (2 Fe at M1 site and one Fe in M2 site). Oxygen atoms are omitted because they are not visible in

447 Z-contrast images due to the weak intensity with respect to Fe and Si. The Fe atoms at M1, M2
448 sites, and Si atoms are colored in yellow, orange, and blue, respectively.
449
450
451 Figure 4: a [100]-zone-axis HRTEM image showing an interface between fayalite (Fa) and 2-
452 layer laihunite (2M). FFT patterns from the 2M domain (B) and fayalite (C) areas show 001 and
453 003 spots that violate 2-fold screw axis due to the multiple diffraction effect in HRTEM imaging.
454 The two arrows indicate spots from the 2-layer laihunite domain. It should be noted that the FFT
455 pattern from the Z-contrast image of Figure 3 does not show 001 and 003 spots because Z-
456 contrast image uses non-coherent scattered electrons at high angle and eliminates multiple
457 diffraction effect (D).
458
459 Figure 5: A [100]-zone-axis Z-contrast image showing interface between fayalite and laihunte
460 domains with doubled (2) and tripled (1.5) periodicities along the ***c***-axis.
461
462 Figure 6: A [110]-zone-axis Z-contrast image showing intergrowth of 1-layer laihunite (1M), 2-
463 layer laihunite (2M), and 3-layer laihunite (3Or). Inserted in the upper left and lower right
464 comers are FFT patterns from 3-layer laihunite and 1-layer laihunite domains, respectively. An
465 outline box area shows an interface between the1-layer laihunite (1M) and the 3-layer laihunite
466 (3Or).
467
468 Figure 7: Z-contrast images of 1-layer laihunite ([100]-zone-axis) showing positions of high
469 density spots (corresponding to Fe, Si) and low-density sites of vacancies. Noise-filtered image

(lower one) better shows the positions of the atoms and vacancy sites. A unit cell of 1-layer laihunite model with the $[]_{0.5}Fe^{2+}_{0.5}Fe^{3+}SiO_4$ stoichiometry is also overlaid on the image. The Fe atoms at M1, M2 sites, and Si atoms are colored in yellow, orange, and blue, respectively.

Figure 8: A [110]-zone-axis Z-contrast image of 1-layer laihunite (a raw image and a noise-filtered image) showing twinning relationship between the two neighboring 1-layer laihunite domains. M2 sites are brighter than M1 sites due to overlapping of Si and Fe^{3+} in the M2 sites along the [110] direction. It is also possible that a small number of Mg atoms migrated into M1 sites. The twin boundary (TB) is a unit cell of fayalite that was proposed by Fu et al (1982). A unit cell of 1-layer laihunite model with the $[]_{0.5}Fe^{2+}_{0.5}Fe^{3+}SiO_4$ stoichiometry is also overlaid on the image. An outlined area in the upper left corner shows an interface between 1-layer laihunite and 3-layer laihunite. Models for the interface (upper) and twin relationship (lower) are shown on the right hand side of the images. The Fe atoms at M1, M2 sites, and Si atoms are colored in yellow, orange, and blue, respectively.

Figure 9: [110]-zone-axis Z-contrast image of an area dominated by 3-layer laihunite with domains of 1-layer laihunite (at top) and 2-layer laihunte. FFT pattern from the 3-layer laihunite shows even *00l* spots (*l = 2n, indexing is based on 3-laiyer laihunite setting*). There are two vacancy layers per unit cell along (001). Ideal stoichiometry for the 3-layer laihunite is $[]_{1.0}Fe^{2+}_{3.0}Fe^{3+}_2\,[SiO_4]_3$, that is two 1-layer laihunite units+ one fayalite unit. Both the image and FFT pattern indicate that there is a 2-fold screw axis parallels to the ***c***-axis, and two mirror

planes parallel to (001) within one unit cell at the position of the dashed lines. A projection of 3-layer laihunite structure (Fe and Si atoms only) is also overlaid on the image.

Figure 10: Polyhedral models along the ***a***-axis projection for laihunite-1M (A), laihunite-2M (B), laihunite-3Or (C), and a previously proposed "laihunite-3M" (D) structure for the 3-layer laihunite. The "laihunite-3M" (D) is not a correct model, because it does not fit the observed Z-contrast images. The polyhedral for Fe atoms at M1, M2 sites are colored in yellow and orange, respectively.

Figure 11. Projections of Fe and Si atoms of laihunite-1M, laihunite-2M, laihunite-3Or, and a previously proposed "laihunite-3M." Panels (A) and (B) illustrate projections of the proposed structures along *a*-axis and [110]-zone axis, respectively. The Fe atoms at M1, M2 sites, Si are colored in yellow, orange, and blue, respectively. The O atoms are omitted due to the weak intensity. Fe(III) in M2B sites neighboring vacancy sites are slightly smaller than Fe(II) in Fe2A sites in order to show the difference between them.

Figure 12: (A) A low magnification Z-contrast image showing nano-tunnels or nano-cracks (indicated by arrows) in the laihunite. (B) A HRTEM image showing a magnetite nano-precipitate in a nano- tunnel.

515

516

517

Table 1. Unit cell parameters of 1-layer, 2-layer and 3-layer laihunite structures. The experimental values are measured from electron diffraction and FFT patterns. Values for fayalite are from Fujino et al (1981). Uncertainty for the measured unit cell parameters is about ±0.02 Å.

	Experiment	DFT calculations
Laihunite-1M	4.80 Å, 10.20 Å, 1x5.80 Å	4.808 Å, 10.230Å, 1x5.808 Å
Laihunite-3Or	4.81 Å,10.25 Å, 3x5.85 Å	4.824 Å, 10.291 Å, 3x5.882 Å
Laihunite-2M	4.82 Å, 10.30 Å, 2x5.93 Å	4.826 Å, 10.319 Å, 2x5.931 Å
Fayalite	4.8195 Å, 10.4788 Å, 6.0873 Å	

Table 2 Structural formulae for fayalite and laihunite domains

Structural formula	Analyzed domain
$([]_{0.00}\,Fe^{2+}_{1.93}Mg_{0.05}Mn_{0.01}Ca_{0.00}Ni_{0.01})SiO_4$	fayalite
$([]_{0.21}\,Fe^{2+}_{1.28}Fe^{3+}_{0.42}Mg_{0.07}Mn_{0.00}Ca_{0.01}Ni_{0.01})SiO_4$	2-layer laihunite
$([][_{0.21}Fe^{2+}_{1.28}Fe^{3+}_{0.43}Mg_{0.06}Mn_{0.01}Ca_{0.00}Ni_{0.01})SiO_4$	2-layer laihunite
$([]_{0.22}Fe^{2+}_{1.28}Fe^{3+}_{0.44}Mg_{0.05}Mn_{0.00}Ca_{0.01}Ni_{0.00})SiO_4$	2-layer laihunite
$([]_{0.225}Fe^{2+}_{1.11}Fe^{3+}_{0.45}Mg_{0.06}Mn_{0.01}Ca_{0.00}Ni_{0.00})SiO_4$	2-layer laihunite
$([]_{0.25}Fe^{2+}_{1.15}Fe^{3+}_{0.50}Mg_{0.09}Mn_{0.00}Ca_{0.0}Ni_{0.01})SiO_4$	2-layer laihunite
$([]_{0.25}Fe^{2+}_{1.16}Fe^{3+}_{0.49}Mg_{0.09}Mn_{0.01}Ca_{0.00}Ni_{0.01})SiO_4$	2-layer laihunite
$([]_{0.30}Fe^{2+}_{1.00}Fe^{3+}_{0.60}Mg_{0.08}Mn_{0.01}Ca_{0.01}Ni_{0.00})SiO_4$	3-layer laihunite
$([]_{0.33}Fe^{2+}_{0.91}Fe^{3+}_{0.66}Mg_{0.08}Mn_{0.01}Ca_{0.01}Ni_{0.00})SiO_4$	3-layer laihunite
$([]_{0.34}Fe^{2+}_{0.93}Fe^{3+}_{0.67}Mg_{0.06}Mn_{0.00}Ca_{0.00}Ni_{0.00})SiO_4$	3-layer laihunite
$([]_{0.35}\,Fe^{2+}_{0.84}Fe^{3+}_{0.70}Mg_{0.10}Mn_{0.00}Ca_{0.00}Ni_{0.01})SiO_4$	3-layer laihunite
$([]_{0.35}Fe^{2+}_{0.88}Fe^{3+}_{0.69}Mg_{0.06}Mn_{0.01}Ca_{0.00}Ni_{0.01})SiO_4$	3-layer laihunite
$([]_{0.37}Fe^{2+}_{0.82}Fe^{3+}_{0.74}Mg_{0.07}Mn_{0.00}Ca_{0.00}Ni_{0.00})SiO_4$	3-layer laihunite
$([]_{0.39}Fe^{2+}_{0.75}Fe^{3+}_{0.77}Mg_{0.07}Mn_{0.01}Ca_{0.01}Ni_{0.01})SiO_4$	3-layer laihunite
$([]_{0.47}Fe^{2+}_{0.50}Fe^{3+}_{0.95}Mg_{0.08}Mn_{0.00}Ca_{0.00}Ni_{0.00})SiO_4$	1-layer laihunite
$([]_{0.48}Fe^{2+}_{0.48}Fe^{3+}_{0.96}Mg_{0.08}Mn_{0.00}Ca_{0.00}Ni_{0.00})SiO_4$	1-layer laihunite
$([]_{0.49}Fe^{2+}_{0.49}Fe^{3+}_{0.98}Mg_{0.04}Mn_{0.00}Ca_{0.00}Ni_{0.00})SiO_4$	1-layer laihunite
$([]_{0.51}Fe^{2+}_{0.38}Fe^{3+}_{1.02}Mg_{0.09}Mn_{0.00}Ca_{0.0}Ni_{0.00})SiO_4$	1-layer laihunite
$([]_{0.52}Fe^{2+}_{0.36}Fe^{3+}_{1.04}Mg_{0.07}Mn_{0.00}Ca_{0.00}Ni_{0.00})SiO_4$	1-layer laihunite
$([]_{0.52}Fe^{2+}_{0.36}Fe^{3+}_{1.04}Mg_{0.08}Mn_{0.00}Ca_{0.00}Ni_{0.00})SiO_4$	1-layer laihuite

554

555 Table 3. Fractional coordinates of atoms and vacancies (Vac) in laihunite-1M, laihunite-2M, and

556 laihunite-3Or structures based on fayalite setting.

Laihunite-1M							
Space group $P2_1/b$			$\alpha = 91.39^\circ$, $\beta=90^\circ$, $\gamma=90^\circ$				
Atom	**x**	**y**	**z**	**Atom**	**x**	**y**	**z**
Fe1	0.00000	0.00000	0.00000	Fe2	0.50625	0.22833	0.25940
Si1	0.56010	0.09479	0.74789	Vac	0.00000	0.00000	0.50000
O1	0.22426	0.10578	0.76075	O2	0.32784	0.05564	0.24005
O3	0.70433	0.17868	0.53945	O4	0.72661	0.17100	0.96877

557

558

Laihunite-2M							
Space group $P2_1/b$			$\alpha = 90.79^\circ$, $\beta=90^\circ$, $\gamma=90^\circ$				
Atom	**x**	**y**	**z**	**Atom**	**x**	**y**	**z**
Fe1A	0.00000	0.00000	0.50000	Fe1A	0.50331	0.49330	0.23409
Fe2A	0.01657	0.72036	0.37275	Fe2B	0.50465	0.77065	0.11864
Vac	0.00000	0.00000	0.00000				
Si1	0.57023	0.90246	0.37007	Si2	0.06434	0.59508	0.11892
O1	0.23210	0.90769	0.37049	O2	0.76982	0.10599	0.12715
O3	0.17407	0.44476	0.12487	O4	0.78700	0.54831	0.37052
O5	0.29257	0.17861	0.01647	O6	0.71221	0.83176	0.47971
O7	0.23020	0.66883	0.22619	O8	0.78605	0.32914	0.25917

559

560

561

Laihunite-3Or							
Space group *Pbnm* $\alpha = 90^\circ$, $\beta=90^\circ$, $\gamma=90^\circ$							
Atom	**x**	**y**	**z**	**Atom**	**x**	**y**	**z**
Fe1A	0.50432	0.22994	0.08029	Fe2A	0.01683	0.28260	0.25000
Fe2B	0.99655	0.00782	0.15910	Vac	0.00000	0.00000	0.00000
Si1	0.56779	0.10031	0.25000	Si2	0.43560	0.90602	0.08000
O1	0.22939	0.09520	0.25000	O2	0.73010	0.39511	0.08605
O3	0.17528	0.55647	0.08450	O4	0.20721	0.32165	0.01079
O5	0.22973	0.33279	0.15182	O6	0.71193	0.17355	0.17585
O7	0.28912	0.04515	0.75000				

562

563

564 Table 4. Structural data of Fe-O octahedra in fayalite, laihunite-1M, laihunite-2M, and laihunite-
565 3Or.

	Fayalite	1M	2M		3Or	
M1-O (Å)	2.16	2.15	2.16	2.16	2.16	
Volume of octahedra (Å^3)	12.79	12.38	12.59	12.79	12.58	
Bond length variation	±0.02	±0.02	±0.03	±0.02	±0.02	
M2-O (Å)	2.17(Fe^{2+})	2.04 (Fe^{3+})	2.04 (Fe^{3+})	2.16 (Fe^{2+})	2.04 (Fe^{3+})	2.16 (Fe^{2+})
Volume of octahedra (Å^3)	13.02	10.90	10.89	12.91	10.89	12.90
Bond length variation	±0.04	±0.03	±0.02	±0.04	±0.03	±0.04

566 Structure of fayalite is from Fujino et al. (1981).

567

568

569 Table 5: Difference between Si and Fe in their z coordinates among proposed models of 1-layer laihunite
570 and fayalite.

Authors	Si	Fe2	difference
Fayalite by Fujino et al.,1981	0.25	0.25	0
Ferrifayalite group, 1976	0.2220	0.2730	0.0510
Fu et al., 1982	0.2430	0.2740	0.0310
Tamada et al., 1983	0.2491	0.2579	0.0088
Chatterjee and Saha-Dasgupta, 2010	0.2501	0.2596	0.0095
This study	0.2521	0.2594	0.0073

571

572

573

574

575 **Appendix**

576 Figure A1. Two possible spin configurations in fayalite, modified from Chatterjee and Saha-
577 Dasgupta (2010).

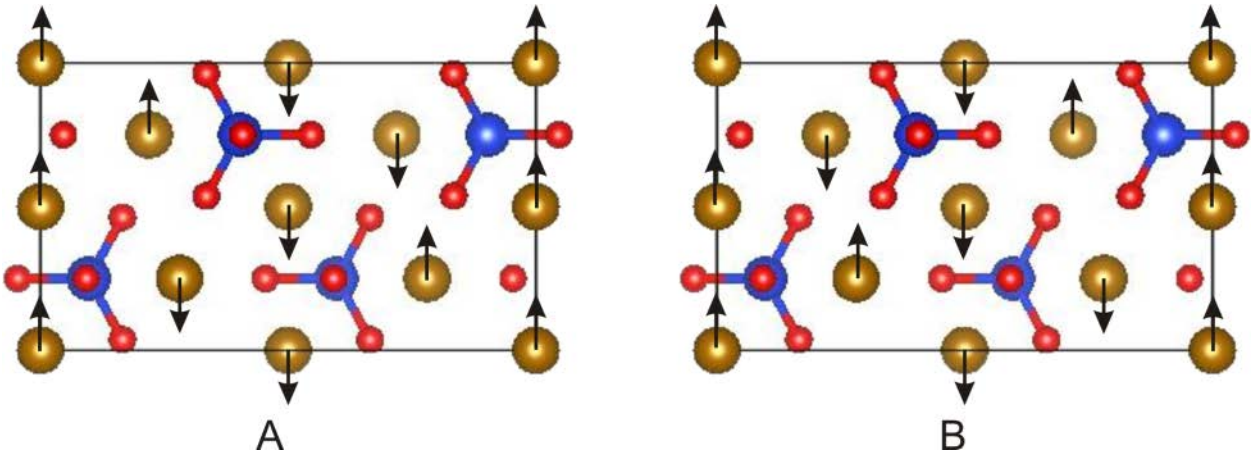

578

579

580 Table A1. Total energy of laihunite-1M, laihunite-2M, and laihunite-3Or in the two possible
581 antiferromagnetic configurations together with fayalite.

Structure	Configuration A (eV)	Configuration B (eV)
Laihunite-1M	-189.79	-189.86
Laihunite-2M	-395.08	-395.21
Laihunite-3Or	-585.00	-585.09
Fayalite	-205.11	-205.17

582

583

584 Figure A2. Simulated electron diffraction patterns of laihunite-2M (A, C) and laihunite-3Or (B,

585 D). A and B are [001]-zone-axis patterns. C and D are [110]-zone-axis patterns.

586

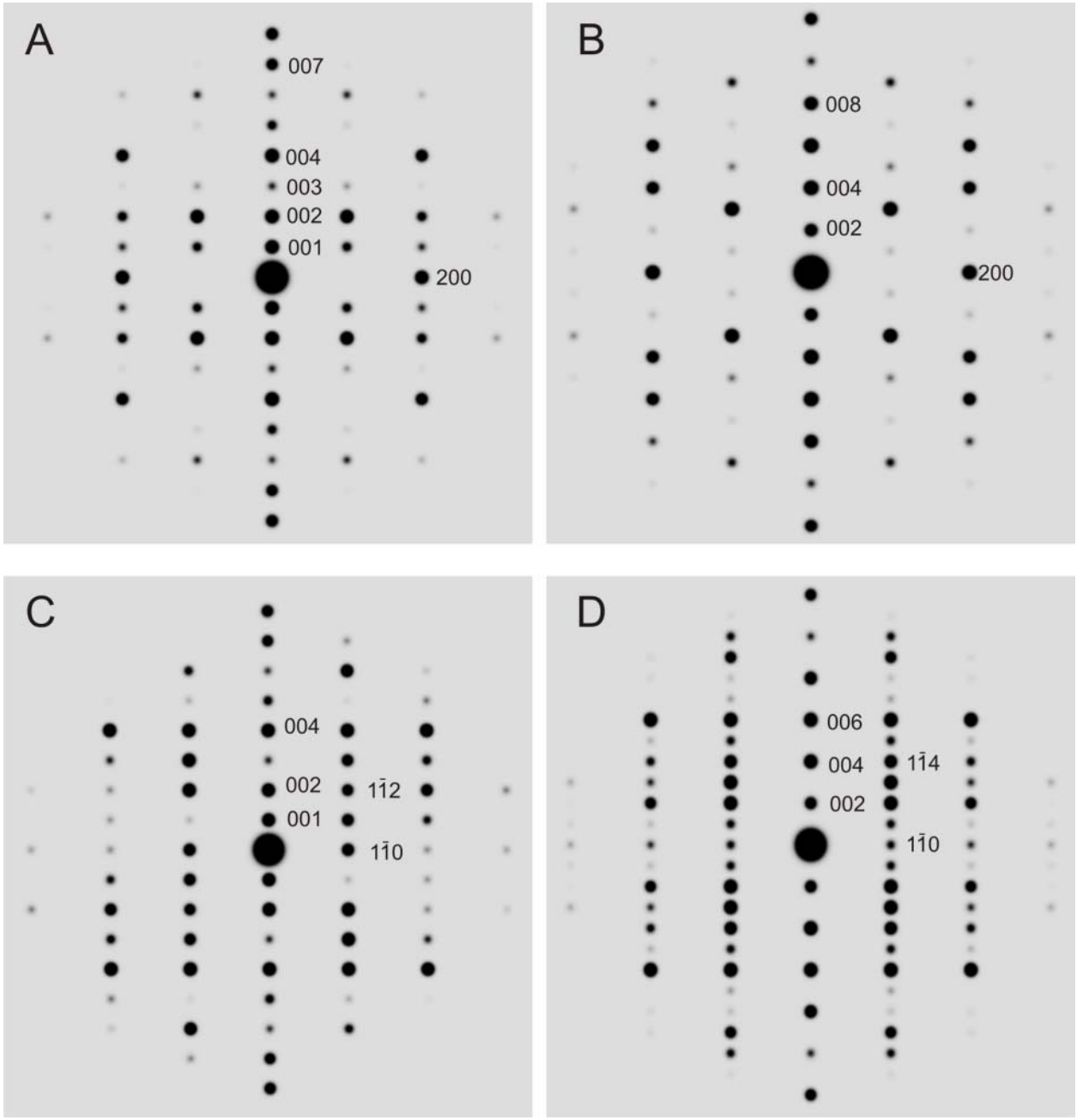

587

Fig. 1

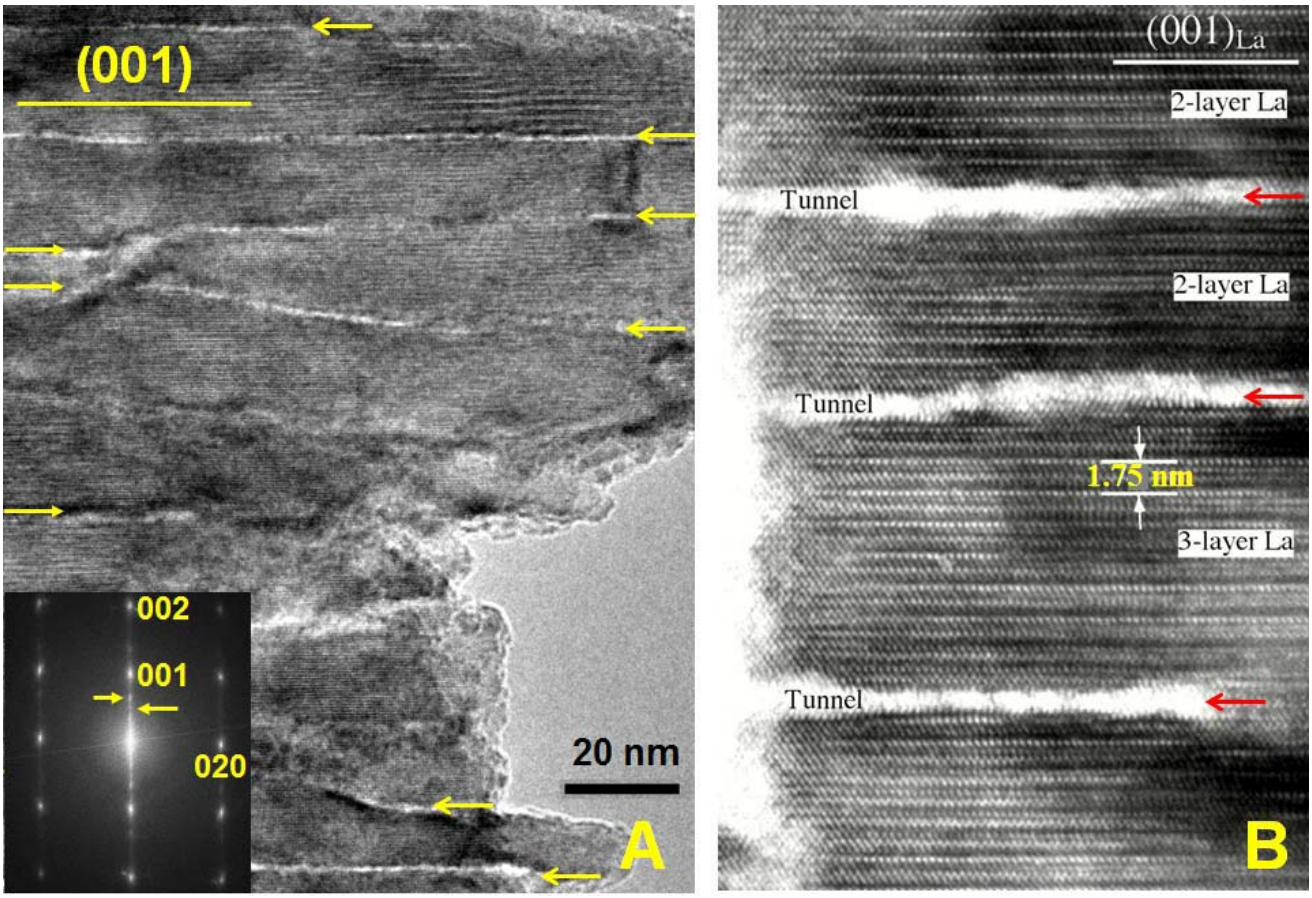
(001)
002
001
020
20 nm
A
(001)La
2-layer La
Tunnel
2-layer La
Tunnel
1.75 nm
3-layer La
Tunnel
B

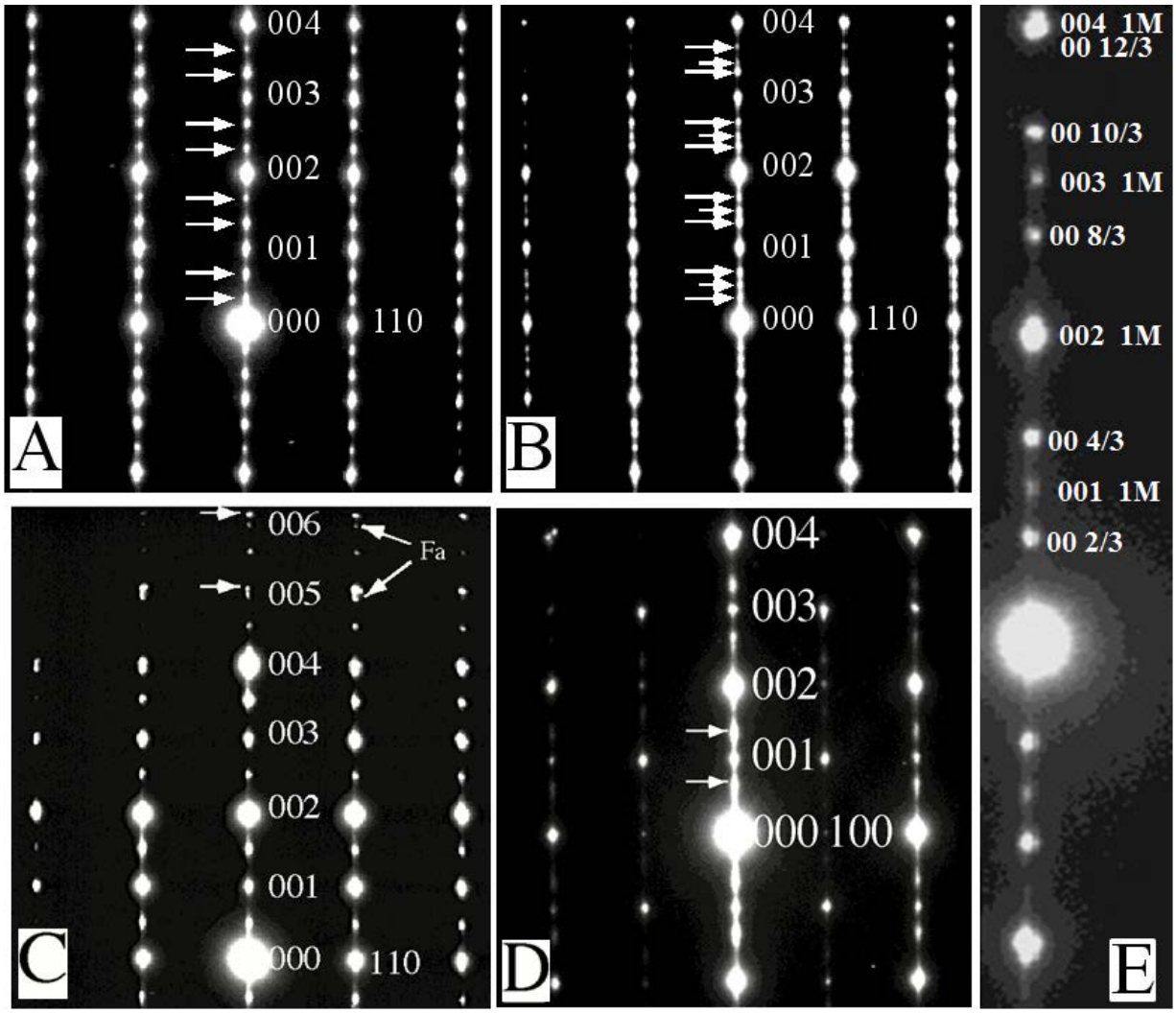
004
003
002
001
000
110
A
004
003
002
001
000
110
B
004 1M
00 12/3
00 10/3
003 1M
00 8/3
002 1M
00 4/3
001 1M
00 2/3
E
006
005
004
003
002
001
000
110
Fa
C
004
003
002
001
000 100
D

Fig. 2

Fig. 3

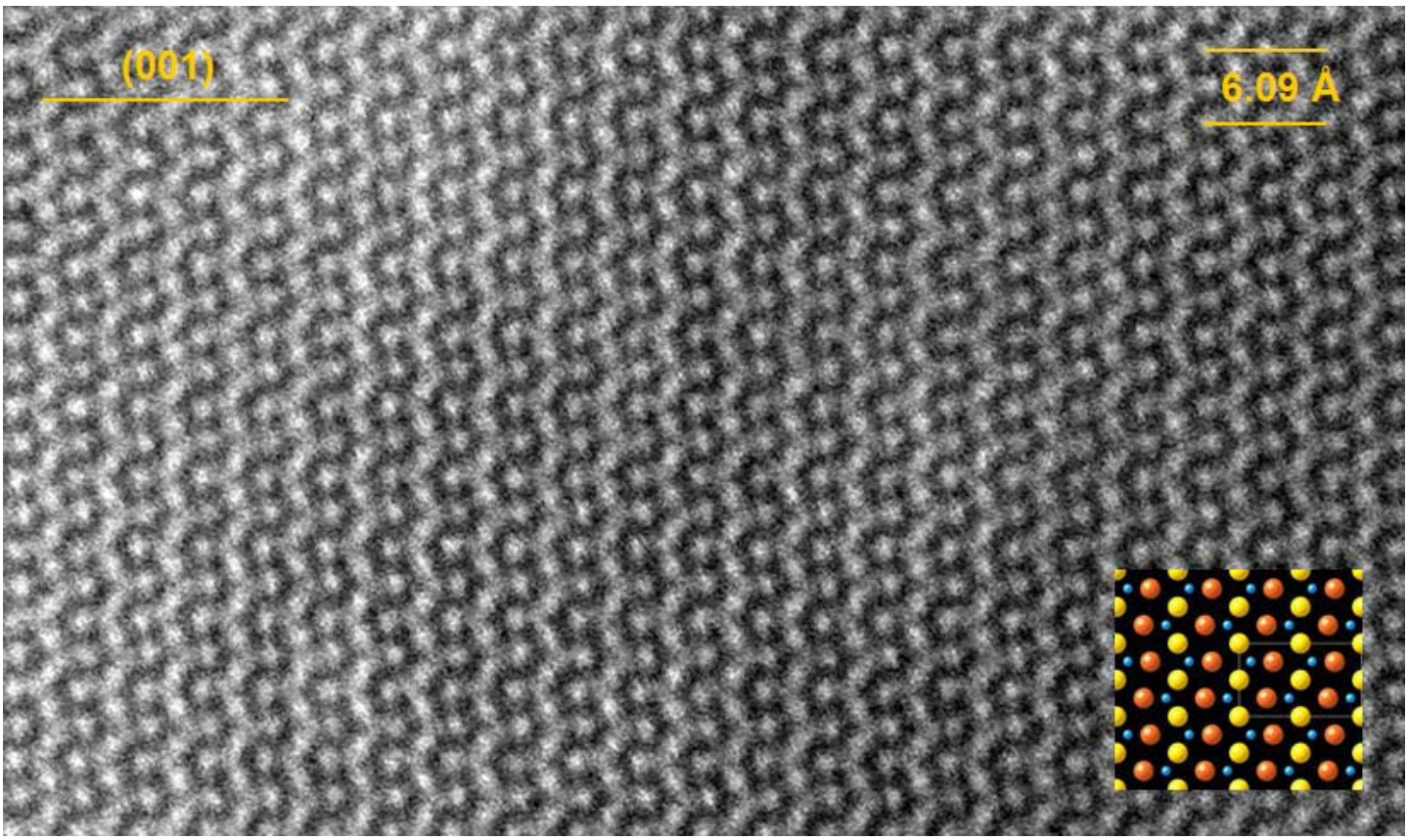

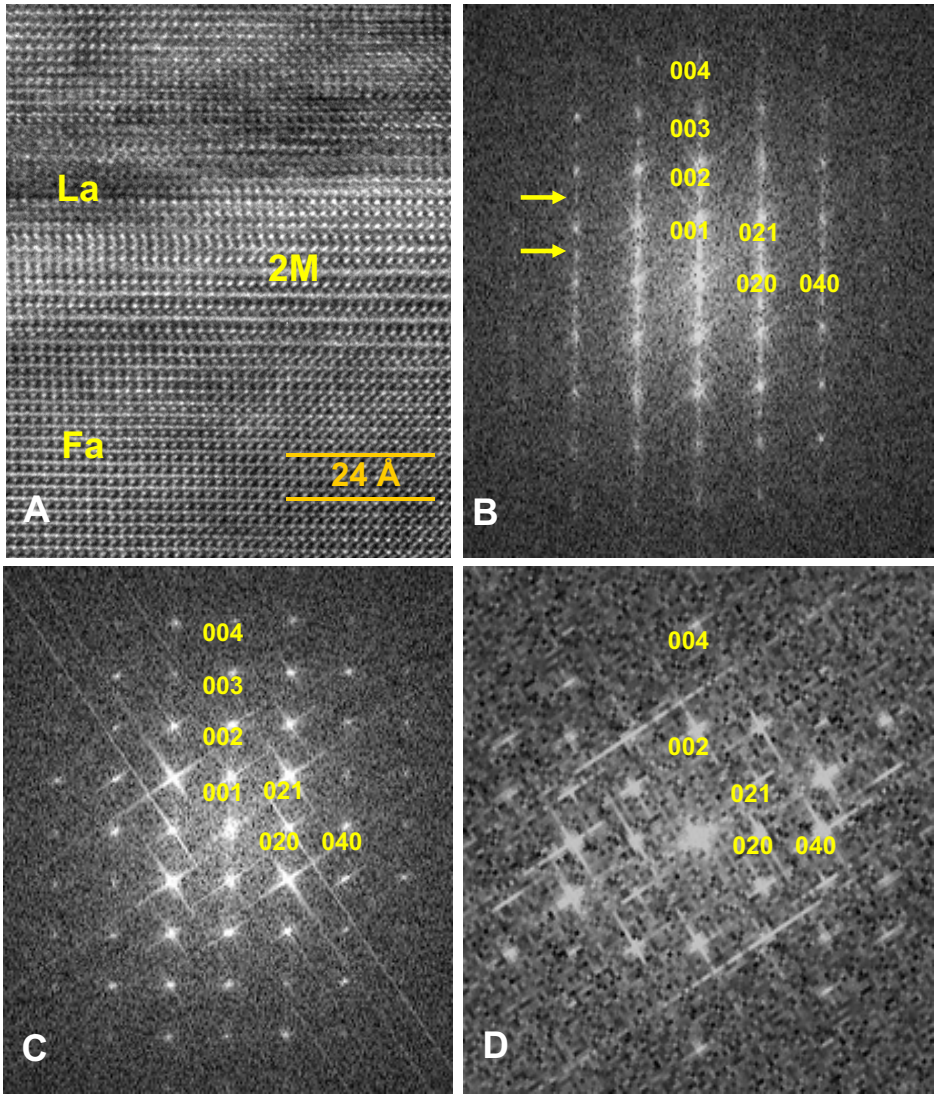
La
2M
Fa
24 Å
A
004
003
002
001
021
020
040
B
004
003
002
001
021
020
040
C
004
002
021
020
040
D

Figure 4

Figure 5

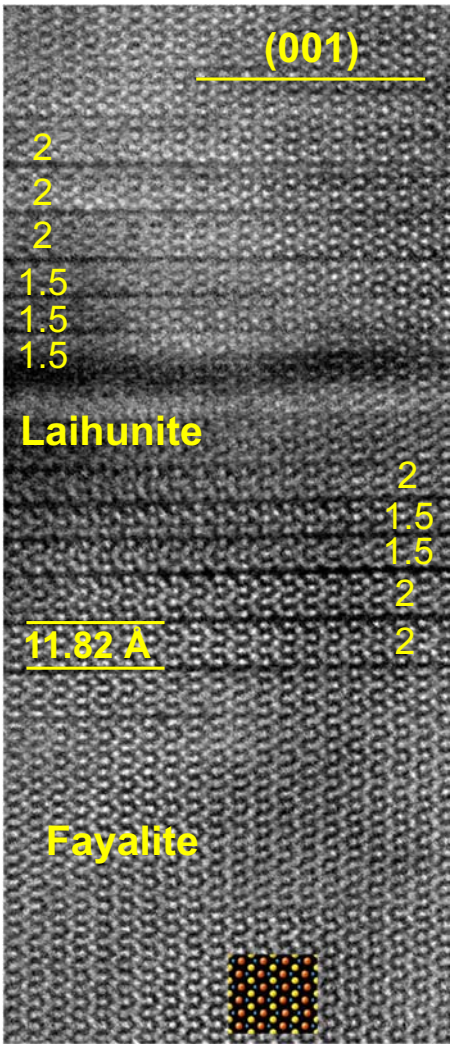

Figure 6

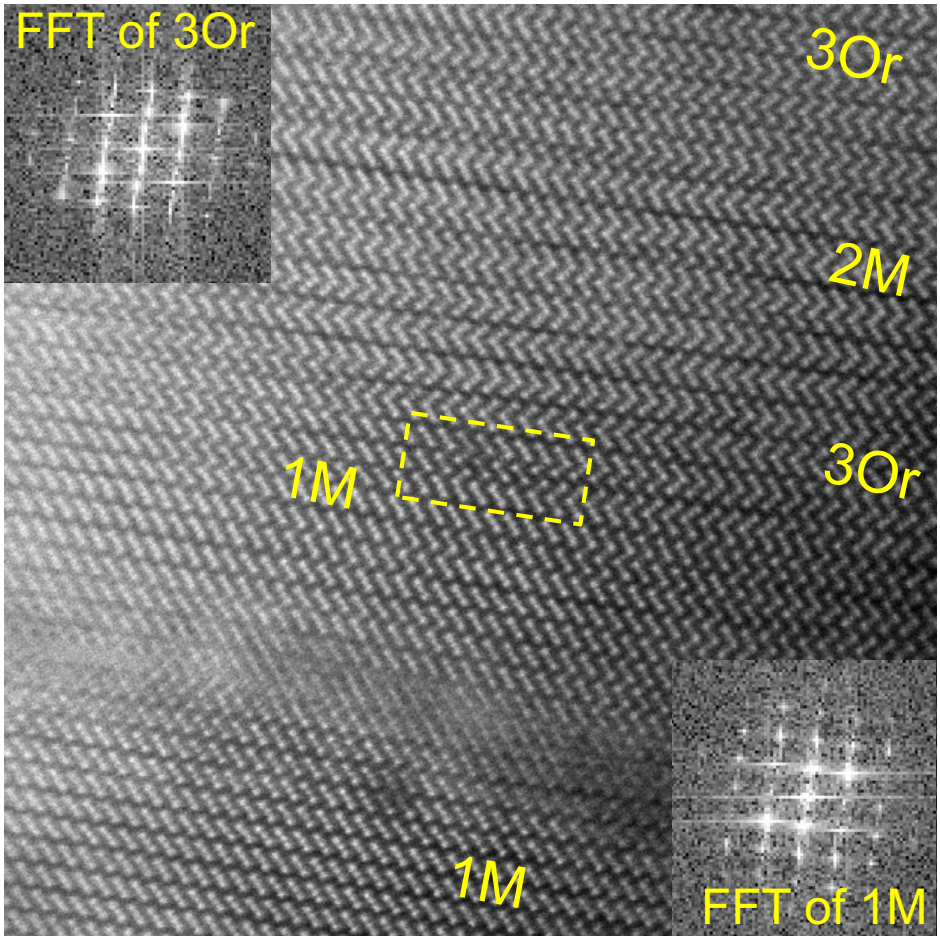

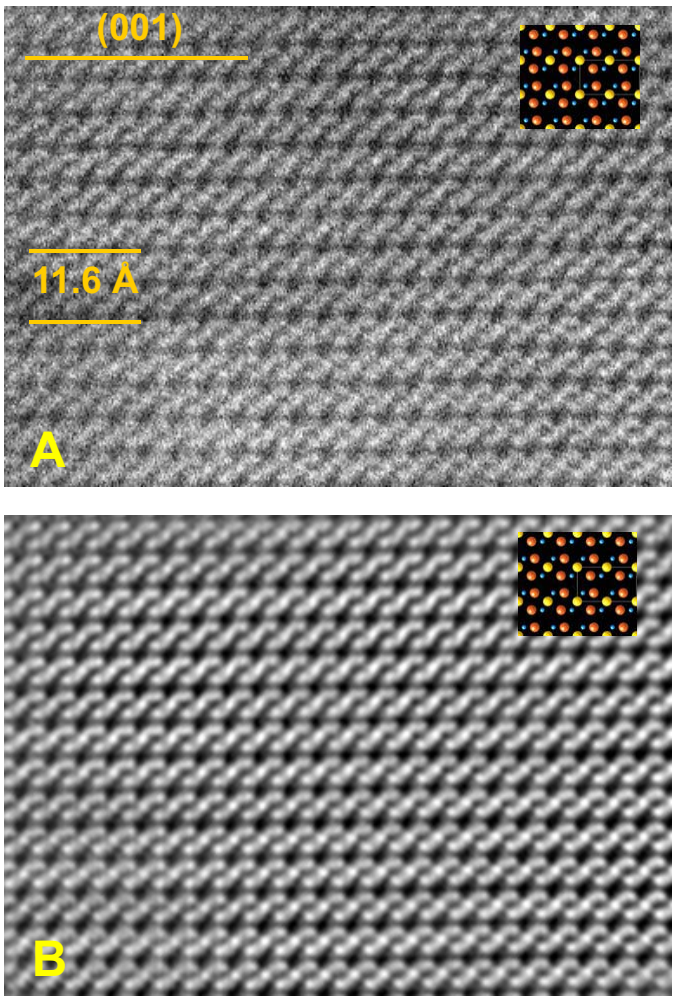

Figure 7

Figure 8

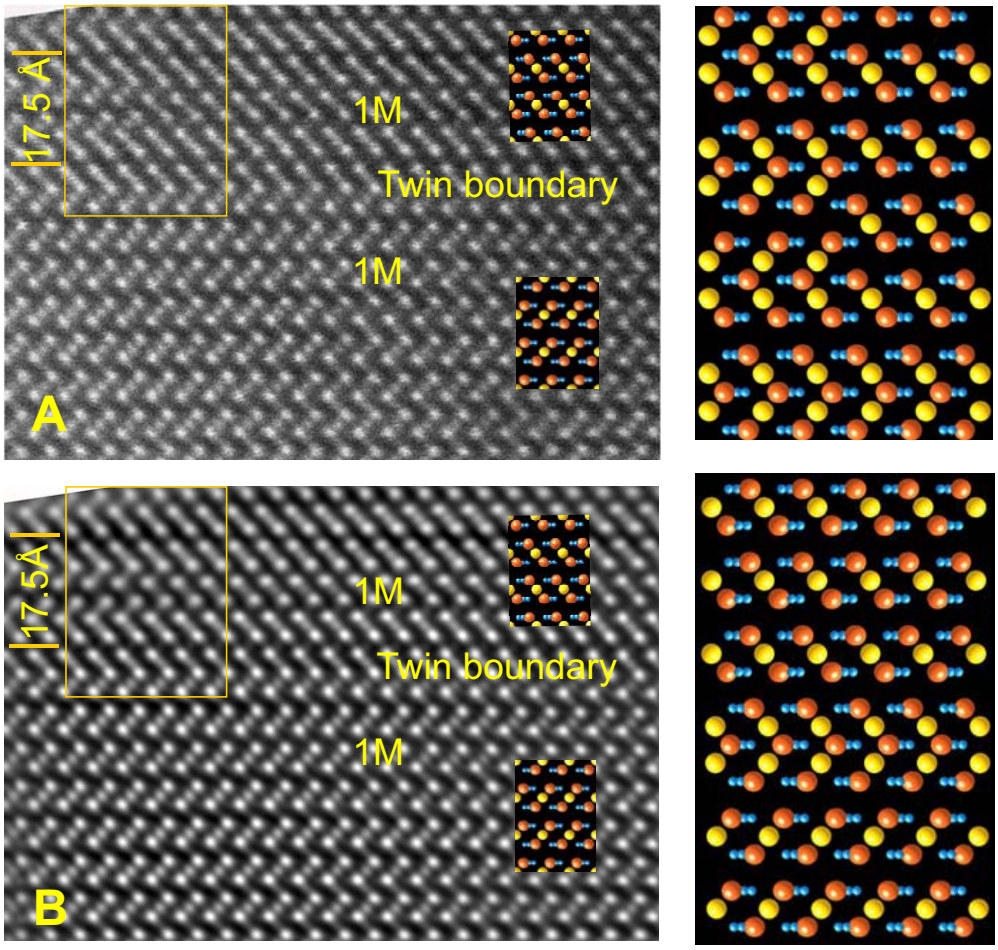

Figure 9

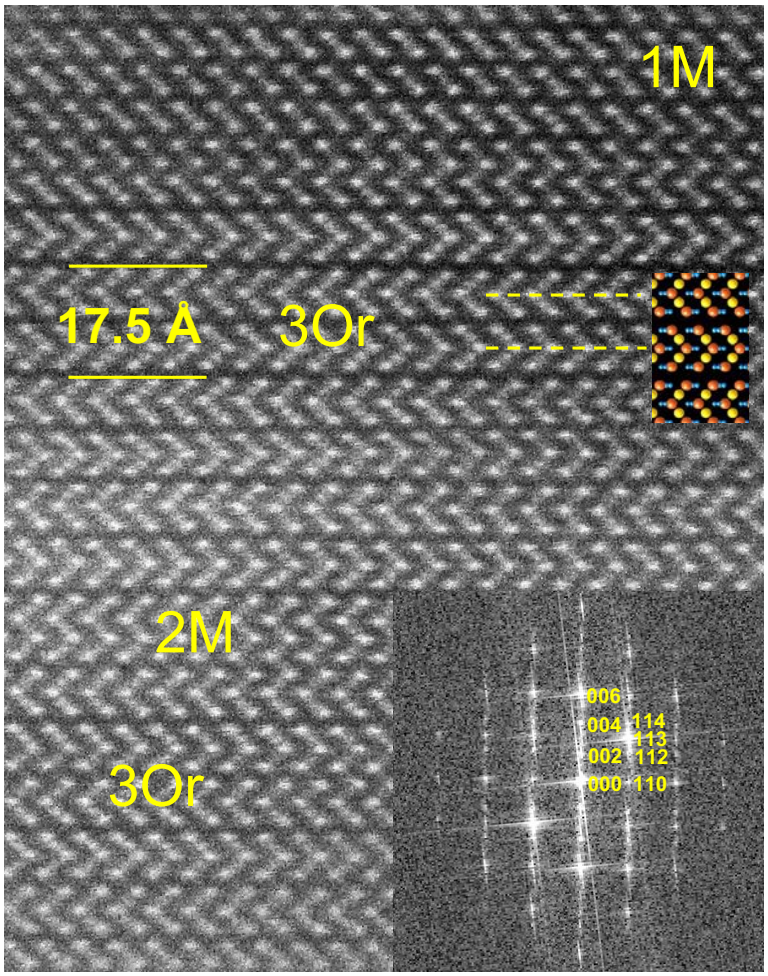

Figure 10

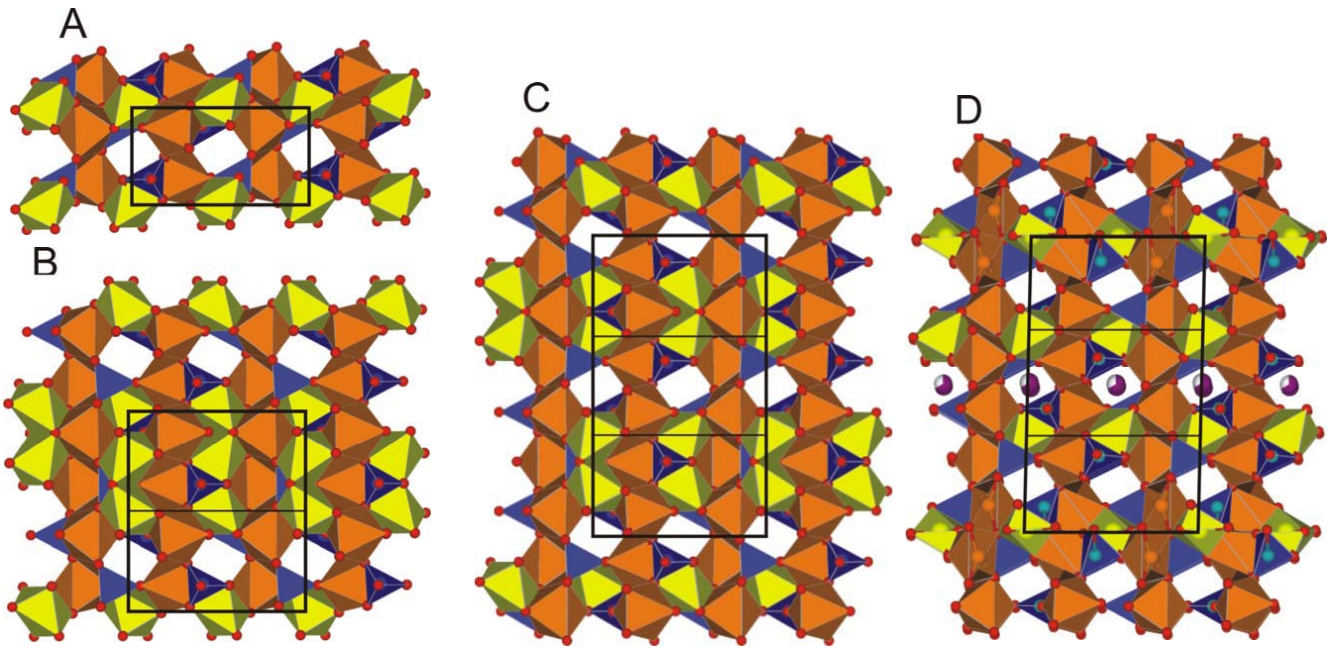

Figure 11

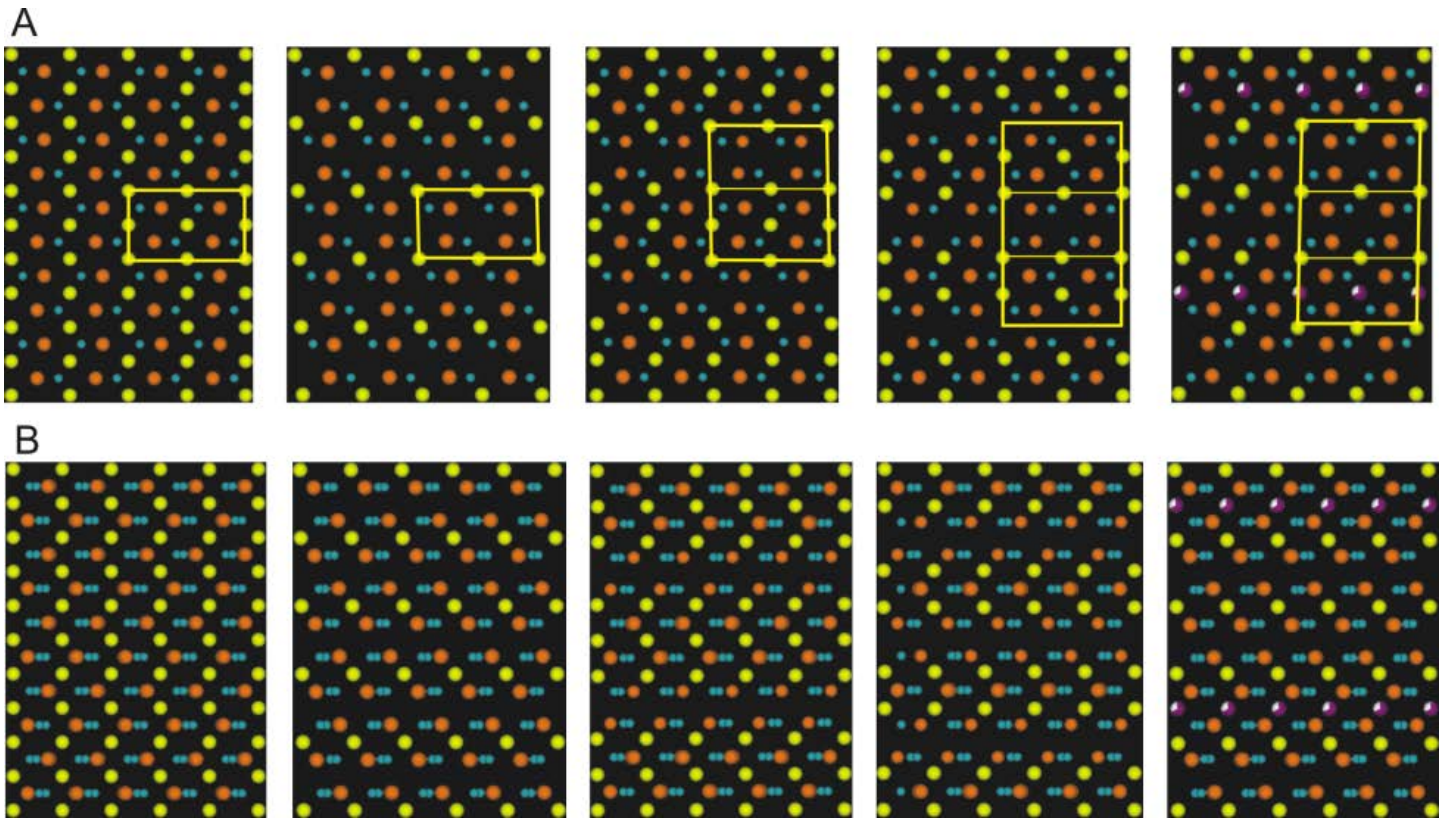
A
B
Fayalite
Laihunite-1M
Laihunite-2M
Laihunite-3Or
“Laihunite-3M”

This is a preprint, the final version is subject to change, of the American Mineralogist (MSA)
Cite as Authors (Year) Title. American Mineralogist, in press.
(DOI will not work until issue is live.) DOI: http://dx.doi.org/10.2138/am.2014.4691

Fig. 12